

N -body simulations using customised potential-density pair basis sets

M.J.W. Brown and J.C.B. Papaloizou

Astronomy Unit, School of Mathematical Sciences, Queen Mary & Westfield College, Mile End Road, London E1 4NS

23 July 2018

ABSTRACT

Potential-density pair basis sets can be used for highly efficient N -body simulation codes, but they suffer from a lack of versatility, i.e. a basis set has to be constructed for each different class of stellar system. We present numerical techniques for generating a biorthonormal potential-density pair basis set which has a general specified pair as its lowest order member. We go on to demonstrate how the set can be used to construct N -body equilibria, which we then evolve using an N -body code which calculates forces using the basis set.

Key words: methods: numerical – celestial mechanics, stellar dynamics – galaxies: kinematics and dynamics.

1 INTRODUCTION

N -body simulations of collisionless stellar systems generally require the evaluation of a smooth gravitational potential from a particle distribution containing fewer particles than stars in the real system by many orders of magnitude. One method for doing this originally proposed by Clutton-Brock (1972,1973) involves the use of a set of basis functions which constitute potential-density pairs. The method has subsequently been used for stability studies of galactic equilibria (e.g. Allen, Palmer & Papaloizou 1990, Hernquist & Ostriker 1992, Earn & Sellwood 1995). The method expands the potential in terms of the specified basis set. The expansion coefficients are evaluated as integrals from the particle distribution which can be regarded as providing a Monte-Carlo estimate for them. The method relies upon the ability to accurately represent the initial equilibrium distribution and its subsequent evolution with the major contribution to the potential coming from the first few members of the basis set. These vary on the global length scale of the entire system and therefore have their expansion coefficients determined most accurately.

Provided the specified basis set retains these advantages during the evolution of the system, the particles used to sample the distribution will evolve in a smooth potential, with the added computational advantage that the N -body problem is reduced to N 1-body problems together with the evaluation of a relatively small number of expansion coefficients.

Earn and Sellwood (1995) performed a stability study of a thin disc in which they made a comparison of normal mode growth rates obtained using simulation techniques with values obtained from a linear perturbation analysis of Kalnajs

(1976). They concluded that the basis function method is the optimal one for the study of the linear growth of instabilities in collisionless equilibria and therefore we suppose small departures from the equilibrium in general. However, they make the comment that the method is very specific. In particular the basis set has to be tailored to the particular density distribution under investigation, which is usually a difficult task and this may create problems when the density distribution changes significantly in a simulation.

Up to now N -body simulations have been performed using basis sets which can be specified analytically and which are based on spherical or thin disc systems, though basis sets for more general axisymmetric systems have been developed (see Robijn & Earn 1996, Earn 1996). In this paper we investigate the possibility of numerically constructing a basis set which can in principle be tailored to any density distribution, although here we focus on axisymmetric systems. The idea is to construct the natural biorthonormal basis for the distribution such that the lowest order member corresponds to a specified system. The basis set is constructed by finding the eigenfunctions of a Fredholm integral equation numerically. These are used to provide the potentials, densities and forces of the basis set on a grid. As an illustration of the method we have determined the basis sets appropriate to a class of perfect oblate spheroids and Kuzmin-Toomre discs. The basis set generation code requires a few hours CPU time to generate 40 basis potential-density pairs and the associated force functions on a dedicated workstation.

As we are interested in general distributions, the equilibria cannot in general be populated with particles by sampling a distribution function as this will be unknown. Instead we use an orbit based method (see Schwarzschild 1979). This populates a time-average distribution of orbits which sam-

arXiv:astro-ph/9806031v1 2 Jun 1998

ples the mass distribution using a quadratic optimisation technique. The subsequent departures from the specified equilibrium and relaxation of the N -body system obtained with evolution under the action of forces computed using the basis set are studied. In general the equilibrium virial ratio is maintained to within two percent using 20K particles and 30 basis functions. Hernquist and Ostriker (1992) noted that discrete particle noise causes particle energies to undergo a random walk and thus leads to a relaxation of the system away from its original configuration. This effect is also studied and found to lead to a relaxation time of roughly order N crossing times. Thus we have found that the basis sets we have constructed can be used effectively in simulations of the axisymmetric equilibria we have considered. They provide a promising tool for problems of stability and other problems where the deviation from the initial configuration is not too large such as finding the response to weak external forcing and we shall report on these in the near future.

In section 2 of this paper we describe the basic theory behind the construction of a customised basis set. In section 3 we present details of the numerical construction of basis sets for two contrasting distributions by two different methods. In section 4 we go on to show how the basis sets can be employed to construct N -body representations of equilibrium stellar systems. In section 5 we evolve the equilibria using an N -body simulation code which uses the appropriate basis set for gravitational force calculation and perform various tests. Finally in section 6 we discuss our results, and outline future work.

2 GENERATING THE BASIS SET

2.1 Theory

Any potential-density pair (Φ_0, ρ_0) satisfies Poisson's equation,

$$\nabla^2 \Phi_0 = 4\pi \rho_0, \quad (1)$$

where we have adopted units such that the gravitational constant $G = 1$. The solution is given by the Poisson integral

$$\Phi_0(\mathbf{r}) = - \int \frac{\rho_0(\mathbf{r}')}{|\mathbf{r} - \mathbf{r}'|} dV'. \quad (2)$$

This and subsequent similar integrals are taken over the volume occupied by the mass distribution.

Equation (2) can be rewritten as:

$$\Phi_0(\mathbf{r}) = \int K(\mathbf{r}, \mathbf{r}') w(\mathbf{r}') \Phi_0(\mathbf{r}') dV', \quad (3)$$

where the weight $w(\mathbf{r})$ is given by

$$w(\mathbf{r}) = - \frac{\rho_0(\mathbf{r})}{\Phi_0(\mathbf{r})}, \quad (4)$$

and the kernel $K(\mathbf{r}, \mathbf{r}')$ by

$$K(\mathbf{r}, \mathbf{r}') = \frac{1}{|\mathbf{r} - \mathbf{r}'|}. \quad (5)$$

Note that for an equilibrium (Φ_0, ρ_0) pair, $w(\mathbf{r})$ is positive definite which is guaranteed for a density that is positive everywhere. This is necessary for the method given below to work. From (3) it follows that

$$\xi_0(\mathbf{r}) = \int \overline{K}(\mathbf{r}, \mathbf{r}') \xi_0(\mathbf{r}') dV', \quad (6)$$

where

$$\xi_0(\mathbf{r}) = \sqrt{w(\mathbf{r})} \Phi_0(\mathbf{r}), \quad (7)$$

and the symmetric kernel

$$\overline{K}(\mathbf{r}, \mathbf{r}') = \sqrt{w(\mathbf{r})w(\mathbf{r}')} K(\mathbf{r}, \mathbf{r}'). \quad (8)$$

This means that ξ_0 is an eigenfunction of the eigenvalue problem defined by the Fredholm integral equation (for a detailed explanation of the properties of this type of eigenvalue problem that we use below see Courant & Hilbert, 1955, ch. 3),

$$\lambda_k \xi_k(\mathbf{r}) = \int \overline{K}(\mathbf{r}, \mathbf{r}') \xi_k(\mathbf{r}') dV', \quad (9)$$

with eigenvalue $\lambda_0 = 1$. Given the eigenfunctions $\{\xi_k\}$ we can calculate the $\{\Phi_k\}$ via (7), and the corresponding $\{\rho_k\}$ are given by

$$\lambda_k \rho_k(\mathbf{r}) = -\Phi_k(\mathbf{r}) w(\mathbf{r}). \quad (10)$$

The variational properties of the eigenvalue problem, taken together with the fact that $\overline{K}(\mathbf{r}, \mathbf{r}')$ is always positive, guarantee that the lowest order eigenfunction which is associated with the largest eigenvalue does not change sign and is therefore ξ_0 . The largest eigenvalue is $\lambda_0 = 1$ and $\lambda_k \rightarrow 0$ for $k \rightarrow \infty$. We define an inner product

$$\langle \Phi_k, \rho_l \rangle = - \int \Phi_k(\mathbf{r}) \rho_l(\mathbf{r}) dV. \quad (11)$$

Then, when suitably normalised, the eigenfunctions obey a biorthonormality relation

$$\langle \Phi_k, \rho_l \rangle = \delta_{kl}. \quad (12)$$

The completeness properties of eigenfunction expansions of the type we consider described in Courant & Hilbert (1955) chapters 3 and 5, indicate that the set is able to represent uniformly and absolutely any potential Φ derived from the Poisson integral applied to a continuous density distribution that vanishes sufficiently rapidly at large distances. Thus

$$\Phi(\mathbf{r}) = \sum_k c_k \Phi_k(\mathbf{r}), \quad (13)$$

where

$$c_k = \langle \Phi_k, \rho \rangle = \langle \Phi, \rho_k \rangle. \quad (14)$$

which is all that is needed for application to N -body calculations. Also we have the formal expansion for the density

$$\rho(\mathbf{r}) = \sum_k c_k \rho_k(\mathbf{r}), \quad (15)$$

Thus given a density ρ we can obtain the corresponding Φ , and vice versa.

2.2 Numerical solution of the eigenvalue problem

Generally equation (9) will not have an analytic solution and therefore numerical methods are required. We work in cylindrical polar coordinates (R, z, ϕ) . Although in principle there are no symmetry restrictions on the equilibrium pair

(Φ_0, ρ_0) , we shall in this paper assume them to be independent of ϕ . Then the equilibrium is axisymmetric and the basis set can be separated into subsets with harmonic azimuthal dependence associated with a particular azimuthal mode number m . Thus we seek a representation of a given potential-density pair as follows;

$$\rho(R, z, \phi) = \sum_{l,m} \rho_{lm}(R, z) \{c_{lm} \cos m\phi + d_{lm} \sin m\phi\},$$

$$\Phi(R, z, \phi) = \sum_{l,m} \Phi_{lm}(R, z) \{c_{lm} \cos m\phi + d_{lm} \sin m\phi\}. \quad (16)$$

That is, for a given m we require basis pairs $(\Phi_{lm}, \rho_{lm})e^{im\phi}$ $l = 0, 1, 2, \dots$ which satisfy (9), with a different weight function $w_m = -\rho_{0m}/\Phi_{0m}$ for each value of m .

We wish the lowest order pair (Φ_{00}, ρ_{00}) to correspond to the axisymmetric equilibrium. Thus we take $\rho_{00} \equiv \rho_0$ to be the equilibrium density.

To derive suitable $\{\rho_{0m} : m \geq 1\}$ we begin by noting that Poisson's equation for the axisymmetric equilibrium distribution is

$$\frac{\partial^2 \Phi_{00}}{\partial R^2} + \frac{1}{R} \frac{\partial \Phi_{00}}{\partial R} + \frac{\partial^2 \Phi_{00}}{\partial z^2} = 4\pi \rho_{00}. \quad (17)$$

Differentiating with respect to R gives

$$\frac{\partial^2}{\partial R^2} \left(\frac{\partial \Phi_{00}}{\partial R} \right) + \frac{1}{R} \frac{\partial}{\partial R} \left(\frac{\partial \Phi_{00}}{\partial R} \right) + \frac{\partial^2}{\partial z^2} \left(\frac{\partial \Phi_{00}}{\partial R} \right) - \frac{1}{R^2} \frac{\partial \Phi_{00}}{\partial R} = 4\pi \frac{\partial \rho_{00}}{\partial R}, \quad (18)$$

but this implies

$$\left(\frac{\partial^2}{\partial R^2} + \frac{1}{R} \frac{\partial}{\partial R} + \frac{\partial^2}{\partial z^2} + \frac{1}{R^2} \frac{\partial^2}{\partial \phi^2} \right) \left(\frac{\partial \Phi_{00}}{\partial R} e^{i\phi} \right) = 4\pi \frac{\partial \rho_{00}}{\partial R} e^{i\phi}. \quad (19)$$

Hence $\left(\frac{\partial \Phi_{00}}{\partial R}, \frac{\partial \rho_{00}}{\partial R} \right) e^{i\phi}$ is a potential-density pair with the ϕ dependence required of a dipole ($m = 1$) term in (16). It corresponds to a small translation of the system. Appropriate higher order (Φ_{0m}, ρ_{0m}) can be obtained after further differentiation with respect to R . One finds that a potential-density pair generated from (Φ_{00}, ρ_{00}) is $\left(R^m \left(\frac{\partial^m}{\partial y^m} \Phi_{00} \right), R^m \left(\frac{\partial^m}{\partial y^m} \rho_{00} \right) \right) e^{im\phi}$, where $y = R^2$. Functions derived in this way can be used to specify a pair (Φ_{0m}, ρ_{0m}) provided these are both of uniform sign as is the case for the examples considered below. But note that the procedure can also be applied to every member of a basis set for $m = 0$ to generate a basis set for any non-zero m .

We present two alternative methods for solving the eigenvalue problem given by equation (9). The first, method a), involves discretising the eigenvalue problem onto a grid and calculating the integral of (9) via direct summation, whilst the second, method b) uses a basis set built from standard orthogonal polynomials to represent the eigenvalue problem, the integration being calculated via Gaussian quadrature. Method a) has the advantage of in general being more accurate for a given amount of computer time, but method b) has more flexibility.

2.3 Basis set generation via direct summation

We seek to numerically evaluate (2) using the $\{\rho_{0m} e^{im\phi}\}$ as the density source terms. Because of the simple ϕ dependence

the ϕ integration can be expressed as a function of elliptic integrals, leaving

$$\Phi_{0m}(R, z) = - \int_{R'=0}^{R'=\infty} \int_{z'=-\infty}^{z'=\infty} \frac{F_m(k^2)}{\sqrt{(R+R')^2 + (z-z')^2}} \times \rho_{0m}(R', z') R' dR' dz', \quad (20)$$

where

$$k^2 = \frac{4RR'}{(R+R')^2 + (z-z')^2}, \quad (21)$$

and

$$F_m(k^2) = 4 \int_0^{\pi/2} \frac{e^{2im\phi} d\phi}{(1-k^2 \cos^2 \phi)^{1/2}}. \quad (22)$$

The (R', z') integration is done by finite summation approximation on an $n \times n$ (R_i, z_j) grid, i.e.

$$[\Phi_{0m}]_{ij} = K_{ijpq} [\Sigma_{0m}]_{pq}, \quad (23)$$

where the summation convention is assumed, and

$$\begin{aligned} [\Phi_{0m}]_{ij} &= \Phi_{0m}(R_i, z_j), \\ K_{ijpq} &= \frac{-F_m(k_{ijpq}^2)}{\sqrt{(R_i + R_p)^2 + (z_j - z_q)^2}}, \\ k_{ijpq}^2 &= \frac{4R_i R_p}{(R_i + R_p)^2 + (z_j - z_q)^2}, \\ [\Sigma_{0m}]_{pq} &= \rho_{0m}(R_p, z_q) R_p dR_p dz_q, \\ dR_p &= \frac{1}{2}(R_{p+1} - R_{p-1}), \\ dz_q &= \frac{1}{2}(z_{q+1} - z_{q-1}). \end{aligned} \quad (24)$$

The contribution to the integral of a cell in which $\mathbf{r} = \mathbf{r}'$ is approximated by setting the value of the kernel in the cell to be the average value of the kernel in the four nearest neighbouring cells.

In practice, especially when equilibria are not bounded in space, it is necessary to transform coordinates from the (R, z) to the (u, v) plane, say, where the exact choice of transformation is chosen to achieve maximum accuracy. This leads to an extra Jacobian factor in $[\Sigma_{0m}]_{pq}$, but does not affect the overall technique.

Once this has been done the matrices are manipulated in the same manner as the original functions were in the theoretical case, giving the discrete analogue of (6),

$$\lambda_{0m} [\xi_{0m}]_{ij} = \overline{K}_{ijpq} [\xi_{0m}]_{pq}. \quad (25)$$

By mapping the $n \times n$ grid to a vector with n^2 elements, equation (25) becomes a symmetric matrix eigenvalue problem which can be solved, for example, using a *QL* factorisation algorithm. Thus the values of the first $n \times n$ eigenfunctions on the coordinate grid are obtained, which can then be used for interpolation.

The CPU time required to generate 40 basis functions and the associated forces is a few hours on a Sun Sparc20 workstation, which is small in comparison to the time required to conduct large long-term simulations. This suggests that it may be possible to generate a new basis set midway through the simulation, if the system under study has evolved away from its initial state to such an extent that the old basis set is no longer able to accurately represent it.

2.4 Basis set generation via Legendre polynomials and Gaussian quadrature

The eigenvalue problem defined by (9) can be expressed in matrix form using a polynomial basis. To do this we suppose a coordinate transformation that maps the cylindrical coordinates (R, z) to (u, v) . This is such that the infinite domain $0 < R < \infty, -\infty < z < \infty$ is mapped into the finite domain $u_1 < u < u_2, v_1 < v < v_2$. For examples see below. We now introduce the orthonormal polynomials

$$\mathcal{P}_{ll'}(\mu_u, \mu_v) = N_{ll'}^{-1/2} P_l(\mu_u) P_{l'}(\mu_v), \quad (26)$$

for $l = 0, 1, 2, \dots, l' = 0, 1, 2, \dots$, where P denotes the Legendre polynomial, with both $\mu_u = \frac{(2u-u_1-u_2)}{(u_2-u_1)}$ and $\mu_v = \frac{(2v-v_1-v_2)}{(v_2-v_1)}$ both lying in $(-1, 1)$. Here the normalization constant $N_{ll'} = (v_2 - v_1)(u_2 - u_1)/((2l+1)(2l'+1))$. These polynomials form an orthonormal basis over the (u, v) domain.

To obtain a matrix eigenvalue problem we first expand (e.g. for $m = 0$) the eigenfunction ξ_{k0} in the form

$$\xi_{k0} = \sum_{ll'} \frac{a_{k,ll'} \mathcal{P}_{ll'}}{\sqrt{|J|}}, \quad (27)$$

where $|J|$ gives the Jacobian such that

$$RdRdz \rightarrow |J|dudv. \quad (28)$$

Then the inner product

$$\langle \xi_{k0}, \xi_{k'0} \rangle = -2\pi \sum_{ll'} a_{k,ll'} a_{k',ll'} = -2\pi \mathbf{a}_k \cdot \mathbf{a}_{k'}, \quad (29)$$

may be written as a scalar product of the column vectors \mathbf{a}_k and $\mathbf{a}_{k'}$ whose components are the expansion coefficients of ξ_{k0} and $\xi_{k'0}$.

Substituting the expansion (27) into the eigenvalue problem defined through (9) and using the orthonormality of the polynomial basis expansion, we obtain the exactly equivalent matrix eigenvalue problem

$$\lambda_k \mathbf{a}_k = \mathbf{M} \cdot \mathbf{a}_k, \quad (30)$$

where the symmetric matrix \mathbf{M} has elements given by

$$\begin{aligned} \mathbf{M}_{ij} = \int \overline{K}(\mathbf{r}, \mathbf{r}') \mathcal{P}_i(u, v) \mathcal{P}_j(u', v') \sqrt{|J|} \sqrt{|J'|} \\ \times d\phi dudvdu'dv'. \end{aligned} \quad (31)$$

Here we have adopted a mapping of the pairs of subscripts associated with the basis functions into single integers i and j and $|J'| = |J(u', v')|$.

Up until now the matrix representation of the eigenvalue problem is exact. Approximations to it are obtained by truncating the polynomial basis such that it becomes finite. Thus we adopt $l = 0, 1, 2, \dots, L_{\max} - 1, l' = 0, 1, 2, \dots, L_{\max} - 1$ giving L_{\max} functions in each of the coordinate directions or L_{\max}^2 in total. Solution of the now finite matrix eigenvalue problem, which can be accomplished with the QL algorithm as above, requires evaluation of the matrix elements given by (31). To do this requires evaluation of multiple integrals. We performed these using Gaussian quadrature in each of the (u, v) coordinate directions using L_{\max} weights. This requires evaluation of the polynomial basis set at the coordinate points corresponding to the zeros of $P_{L_{\max}}(\mu_u)$

and $P_{L_{\max}}(\mu_v)$. These points also provide a natural grid on which to evaluate the eigenfunctions once their expansion coefficients have been found from the solution of the eigenvalue problem. For practical evaluation, the kernel $\overline{K}(\mathbf{r}, \mathbf{r}')$ was of necessity softened for $\mathbf{r} = \mathbf{r}'$ by replacing $|z - z'|$ by $0.05R$ rather than zero. Tests showed results to be independent of the details of the softening.

We found that a successful solution to the eigenvalue problem and construction of the eigenfunctions for the examples given below could be obtained along these lines using black box software found in Press et al. (1996). Comparable results to those obtained with the grid based method, for similar computational overhead, for the low order functions and performance in N -body codes was obtained for $L_{\max} = 30$. Forces could be obtained as described below or by simple low order interpolation and numerical differentiation of the potentials. To conduct simulations using a basis set it is obviously necessary to possess the forces associated with the basis potentials. If the potentials were known analytically, the simplest way to calculate the forces would be via direct differentiation. But because the potentials are known only on a coordinate grid or via polynomial approximation it is more accurate to obtain the forces via integration of the densities over the force kernel, i.e. for the density function $\rho_{lm}(R, z)e^{im\phi}$,

$$\mathbf{F}_{lm}(\mathbf{r}) = e^{im\phi} \int \frac{(\mathbf{r}' - \mathbf{r})e^{im(\phi' - \phi)}}{|\mathbf{r}' - \mathbf{r}|^3} \rho_{lm}(R', z') dV', \quad (32)$$

using the same numerical integration algorithm that was used to calculate the potentials. Hence we obtain the set of forces $\{\mathbf{F}_{lm}\}$ which correspond to the potential-density pair basis set $\{\Phi_{lm}, \rho_{lm}\}$.

3 TWO EXAMPLE BASIS SETS

As illustrations of the technique basis sets have been constructed for two contrasting distributions, the perfect oblate spheroid (POS), and a Kuzmin-Toomre (KT) disc with a Gaussian vertical density profile. Henceforth all results shown were achieved using basis sets generated by method a), though similar results were obtained using functions generated via method b).

3.1 Perfect oblate spheroid

The perfect oblate spheroidal potential (POSP) and its corresponding density are best described in some form of prolate spheroidal coordinates. Details and properties of this distribution can be found in de Zeeuw (1985), and an analytic but non orthonormal set of functions was constructed for application to it by Syer (1995). The choice of coordinates made here for numerical integration purposes was

$$\begin{aligned} z &= \frac{1}{e} \tan u \tan v, \\ R^2 &= \frac{1}{e^2} (\tan^2 u - e^2)(e^2 - \tan^2 v), \\ u &\in [\arctan(e), \pi/2), \\ v &\in [-\arctan(e), \arctan(e)], \end{aligned} \quad (33)$$

where (u, v) are orthogonal coordinates in the (R, z) plane. The parameter e describes the flatness of the distribution

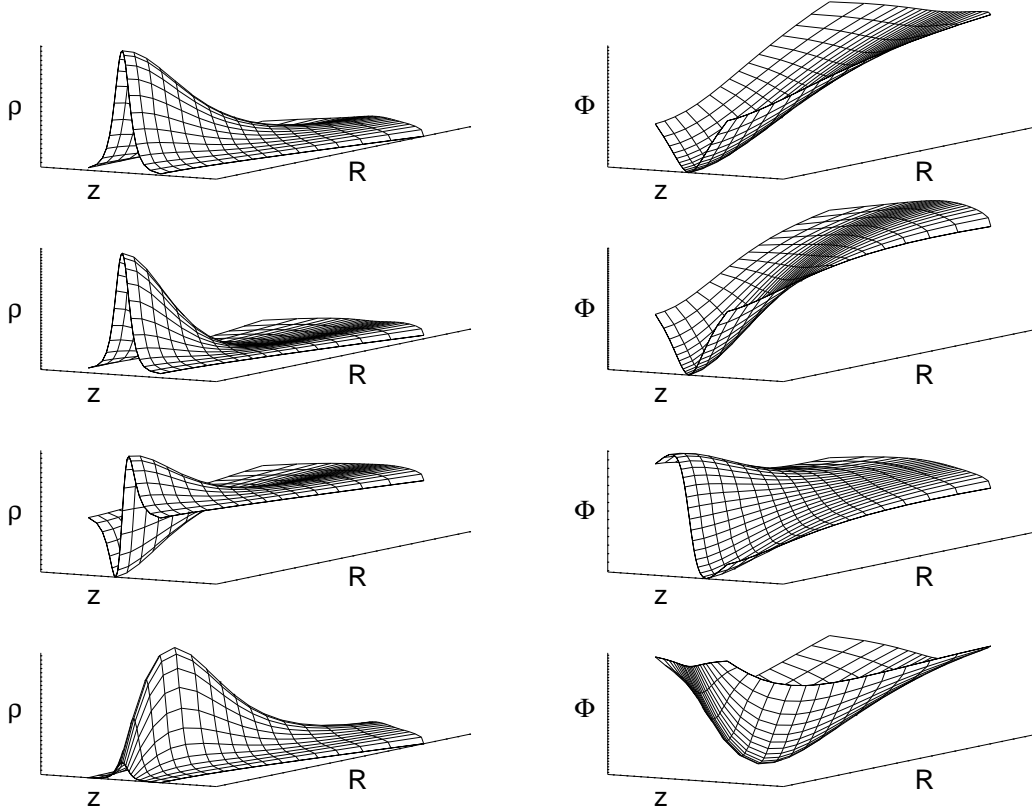


Figure 1. Some example (Φ_{lm}, ρ_{lm}) of the perfect oblate spheroid with $e = 5$. From top to bottom they are $(l, m) = (0, 0), (1, 0), (5, 0), (0, 1)$.

(e.g. $e = 0$ gives a spherical distribution, and the system flattens with increasing e). Lines of constant u give ellipses, lines of constant v give hyperbolae orthogonal to the constant u ellipses and we are only concerned with a finite domain in the (u, v) plane.

The perfect oblate spheroidal density and potential are given by:

$$\rho(u, v) = \frac{e(1 + e^2)}{2\pi} \cos^4 u \cos^4 v \equiv \rho_{00}, \quad (34)$$

$$\Phi(u, v) = \frac{e(u \tan u - v \tan v)}{\tan^2 u - \tan^2 v} \equiv \Phi_{00}. \quad (35)$$

Because the equilibrium potential is known analytically, the numerically obtained $\{\Phi_{0m}\}$ and their corresponding forces can be directly compared with the exact values and the accuracy of the numerical basis function calculation determined. We find that method a) using a 50×50 (u, v) grid is sufficient to produce results with a maximum relative error in the potential of less than 0.2% and in the force of 0.7% over 90% of the mass of the system, whilst method b) using 30×30 Gaussian weights has roughly double the error of the direct method. This level of accuracy is more than sufficient for the

purpose of N -body simulations where particle discreteness of the N -body system is the dominant source of error.

Four of the potential-density pair basis functions for an $e = 5$ perfect oblate spheroid are shown in Figure 1. From top to bottom they are the original distribution, the first radially oscillatory function, the first z oscillatory function, and the first dipole ($m = 1$) function. Having constructed a basis set, we should ensure that the functions are capable of representing the kind of perturbations away from equilibrium that we wish to investigate, using only the first few members of the set. We can illustrate this by representing the following potential (following Syer 1995),

$$\Phi^{\text{pert}}(\mathbf{r}) = \Phi_1(\mathbf{r}, e_1) + \alpha \Phi_2(\mathbf{r}, e_2), \quad (36)$$

where Φ_1 is the POSP that the basis set was based on, with eccentricity e_1 , Φ_2 is the POSP of a different eccentricity e_2 , and α is some positive number less than unity. (The integrations involved in evaluating the expansion coefficients were calculated numerically using the same coordinate grid on which the functions were originally generated). The convergence of the series is demonstrated graphically in Figure 2, for the values $e_1 = 5, e_2 = 2$, and $\alpha = 0.3$. The left plots show successive approximations of the potential and

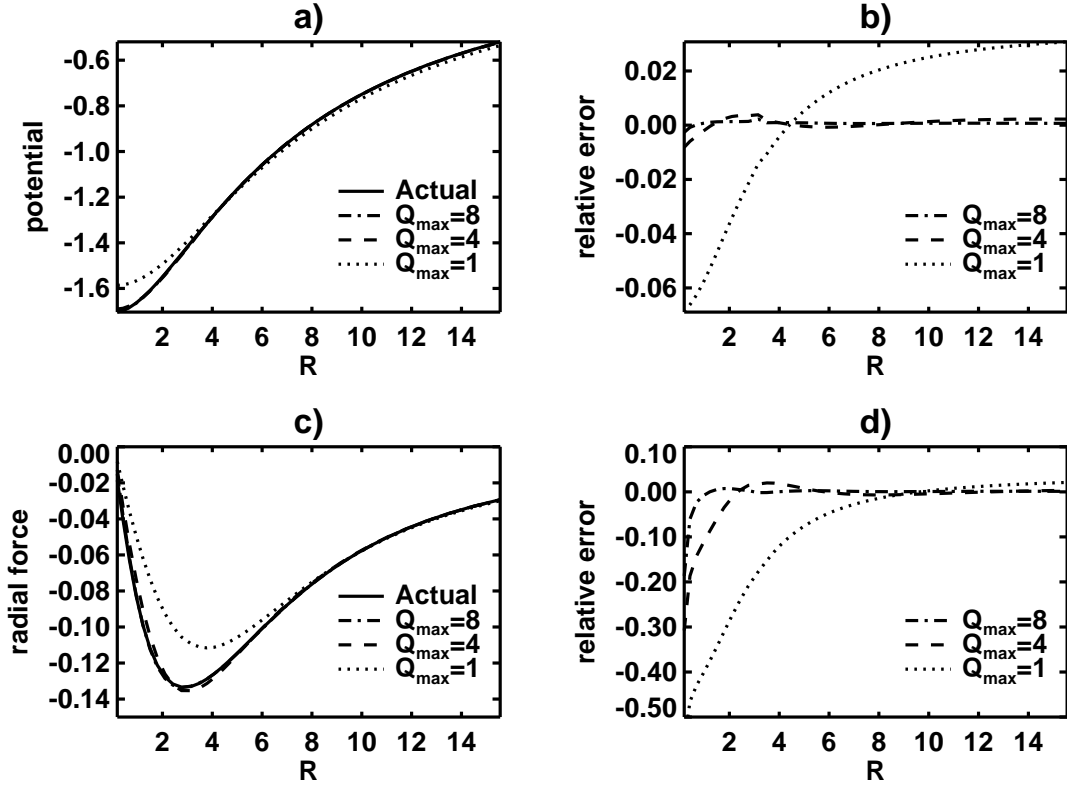


Figure 2. a) shows the basis representation of the potential given in equation (36) in the $z = 0$ plane using upto Q_{\max} basis functions and b) shows the associated relative error, whilst c) and d) are the same plots, for the radial force expansion (for $z = 0$).

radial force in the $z = 0$ plane using one, four, and eight basis functions and the right plots show the corresponding relative error (where we have defined the relative error of a quantity f , say, to be $f_{\text{approx}}/f_{\text{exact}} - 1$).

The high level of accuracy in the expansion representation of the perturbed distribution gives us confidence in the utility of our basis set. (The error in the force expansion at small R is not a problem in practice as the magnitude of the radial force tends to zero at small R and it affects such a small fraction of the total mass of the system).

3.2 Kuzmin-Toomre disc

The Kuzmin-Toomre disc profile with a gaussian vertical density profile (e.g. Sellwood 1994) is given by

$$\rho(R, z) = \frac{\Sigma(R)}{(2\pi)^{1/2} z_0} \exp\left(-\frac{z^2}{2z_0^2}\right) \equiv \rho_{00}, \quad (37)$$

with

$$\Sigma(R) = \frac{M}{2\pi a^2} \left(1 + \frac{R^2}{a^2}\right)^{-3/2}. \quad (38)$$

Again for numerical purposes we make a coordinate transformation in which the domain of interest is finite,

$$\begin{aligned} R &= a \tan(u), \\ z &= \sqrt{2} z_0 \tan(v), \\ u &\in [0, \pi/2), \end{aligned}$$

$$v \in (-\pi/2, \pi/2). \quad (39)$$

The potential of the density given by (37) is not known analytically. However, using a finite difference method on a equally spaced 50×50 (u, v) grid, the potential can be calculated to a specified accuracy. This can be compared with the potential obtained via the approximation (23) calculated on the same (u, v) grid. The maximum relative error is less than 1% over 80% of the mass of the disc using method a), which is acceptable, particularly if the particle discs we use in simulations are truncated at this mass level. Similar accuracy was obtained with method b) with $L_{\max} = 30$. Some members of the set with $z_0 = 0.1$, $a = 1$, $M = 1$ are shown in Figure 3. From top to bottom they are the original distribution, the first radially oscillatory function, the first z oscillatory function, and the first dipole ($m = 1$) function. We note that this system constitutes a severe test of the technique, because of the extreme differences in behaviour in the R and z directions.

4 CONSTRUCTION OF EQUILIBRIUM MODELS

The task is to assign positions and velocities to N discrete particles so that they represent a steady state system described by the potential-density pair (Φ_{00}, ρ_{00}) .

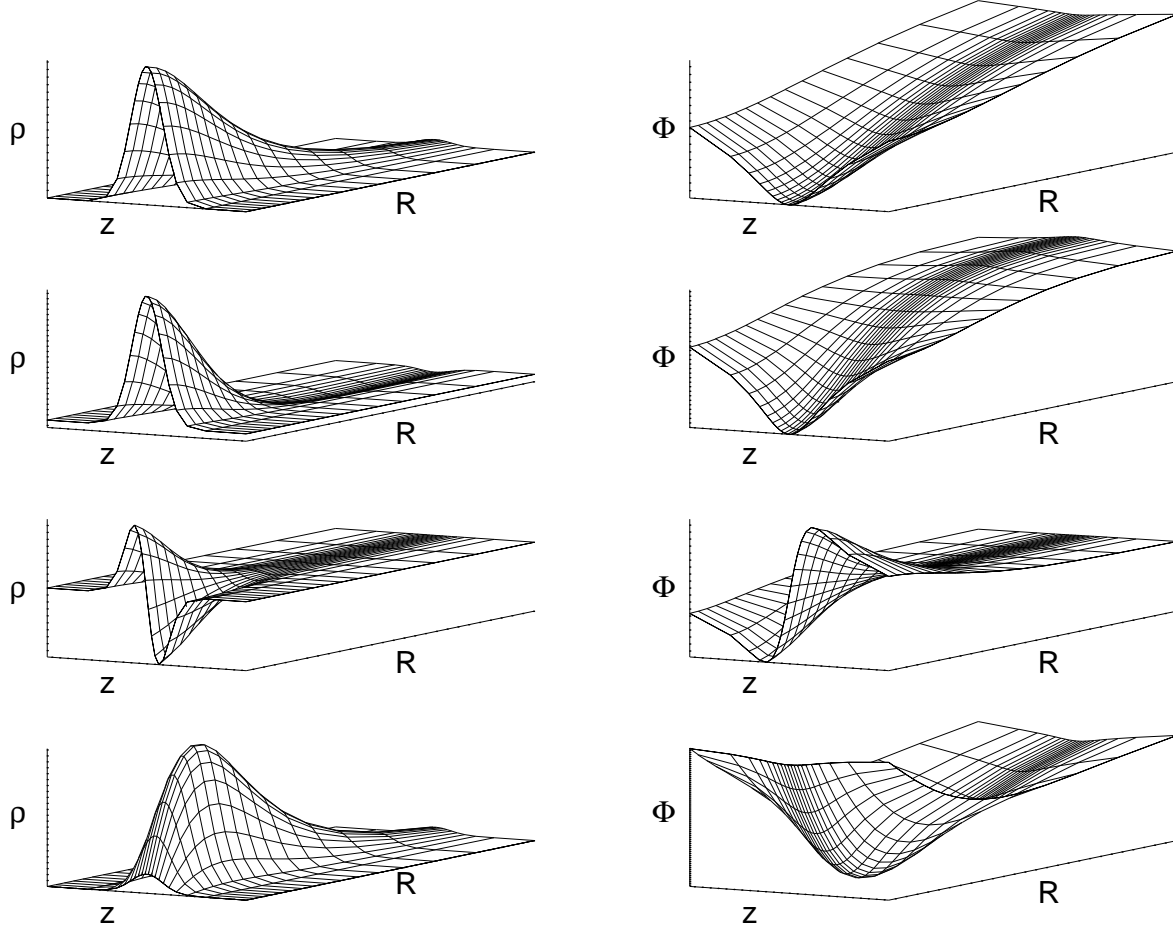


Figure 3. Some example (Φ_{lm}, ρ_{lm}) of the KT disc with $z_0 = 0.1, a = 1, M = 1$. From top to bottom they are $(l, m) = (0, 0), (1, 0), (5, 0), (0, 1)$.

4.1 Orbit representation

The approach we follow is to write the density distribution of the particles as a weighted sum of contributions from M different orbits, that is

$$\rho(\mathbf{r}, t) = \sum_{k=1}^M m_k \delta(\mathbf{r} - \mathbf{r}_k(t)), \quad (40)$$

where each $\mathbf{r}_k(t)$ describes a different orbit labelled with the index k . The total number of particles in each orbit is m_k if each particle has unit mass (as is assumed throughout this paper).

4.2 Fitting the prescribed density

Using the first Q_{\max} axisymmetric members of the basis set constructed earlier, for any density $\rho(\mathbf{r}, t)$ we can construct the quantity

$$D(t) = \langle \Phi_{00} - \sum_{l=0}^{Q_{\max}-1} c_{l0}(t) \Phi_{l0}, \rho_{00} - \sum_{l=0}^{Q_{\max}-1} c_{l0}(t) \rho_{l0} \rangle, \quad (41)$$

where

$$c_{l0}(t) = \langle \Phi_{l0}(\mathbf{r}), \rho(\mathbf{r}, t) \rangle = - \sum_{k=1}^M m_k \Phi_{l0}(\mathbf{r}_k(t)). \quad (42)$$

Using the biorthonormality relation (12), D can be written as:

$$D = 1 - 2c_{00} + \sum_{l=0}^{Q_{\max}-1} c_{l0}^2, \quad (43)$$

We see that D is minimised when $c_{00} = 1$, and $c_{l0} = 0$ for $l \geq 1$.

Because D is non-negative and is zero only when $\rho(\mathbf{r}, t) = \rho_{00}(\mathbf{r}, t)$, we can regard it, in an appropriate norm, as a measure of the ‘distance’ that $\rho(\mathbf{r}, t)$ is ‘away from’ $\rho_{00}(\mathbf{r})$.

Further, as we are seeking a steady state solution which should have a time independent density, we can take a long-time average to remove the explicit t dependence in the coefficients $c_{l0}(t)$. Then we find

$$D = \langle \Phi_{00} - \sum_{l=0}^{Q_{\max}-1} \bar{c}_{l0} \Phi_{l0}, \rho_{00} - \sum_{l=0}^{Q_{\max}-1} \bar{c}_{l0} \rho_{l0} \rangle, \quad (44)$$

where each coefficient is replaced by its time average denoted with an overline

$$\bar{c}_{l0} = \lim_{t \rightarrow \infty} \left\{ \frac{\int_0^t c_{l0}(t) dt}{t} \right\}.$$

In practice we have found that stable time averages can be obtained after following an orbit for a time of order a hundred crossing times for the cases we have considered.

The task is to assign a different mass to each orbit to make the distribution of the particles match ρ_{00} as closely as possible, in a time averaged sense. This can be regarded as being equivalent to minimising D subject to the constraint that $m_k \geq 0$. Using the time averaged coefficients, D can be written as:

$$D = 1 - 2\bar{c}_{00} + \sum_{l=0}^{Q_{\max}-1} \bar{c}_{l0}^2, \quad (45)$$

with

$$\bar{c}_{l0} = - \sum_{k=1}^M m_k \bar{\Phi}_{l0}(\mathbf{r}_k), \quad (46)$$

and

$$\bar{c}_{l0}^2 = \sum_{k,p=1}^M m_k m_p \bar{\Phi}_{l0}(\mathbf{r}_k) \bar{\Phi}_{l0}(\mathbf{r}_p). \quad (47)$$

We may write this in the equivalent form

$$D = 1 + 2\mathbf{m} \cdot \bar{\Phi}_{00} + \mathbf{m} \cdot \mathbf{A} \cdot \mathbf{m}, \quad (48)$$

where the vector components $[\mathbf{m}]_k = m_k$, and $[\bar{\Phi}_{00}]_k = \bar{\Phi}_{00}(\mathbf{r}_k)$, with the matrix element

$$\mathbf{A}_{kp} = \sum_{l=0}^{Q_{\max}-1} \bar{\Phi}_{l0}(\mathbf{r}_k) \bar{\Phi}_{l0}(\mathbf{r}_p), \quad k, p = 1, \dots, M. \quad (49)$$

Thus, to calculate \mathbf{m} in such a way as to provide the closest fit to the specified equilibrium, we have a quadratic optimisation problem, namely to minimise D subject to the constraint $m_k \geq 0, k = 1, \dots, M$.

However there is a further complication, as the number of eigenfunctions used is (usually considerably) smaller than the number of orbits, making the problem ill-conditioned, and the particular method we use to minimise D gives a solution where very few occupation numbers are non-zero. This ill-conditioning can be removed by the use of a profit function. By adding a function to D which is small when the distribution of orbits is smooth, the degeneracy of the solution is removed, and a wider spread of occupation numbers is achieved (For examples, see Richstone & Tremaine 1988, Merritt 1993, Syer & Tremaine 1996). We can interpret the solution to the modified minimisation problem as one which

minimises the deviation from the desired density distribution whilst simultaneously using surplus degrees of freedom manifest in the degeneracy of the pure problem to minimise the profit function.

We note that Tremaine, Hénon & Lynden-Bell (1986) argue that in the presence of small scale mixing, all functions of the form $-\int C(F) dx d\mathbf{v}$, where F is the distribution function and C is any convex function, increase during collisionless relaxation, though in general this conjecture is false (Sridhar 1987). This suggests that we seek a profit function of the form $\sum_{k=1}^M C(m_k)$. In this context, if phase space is divided up into cells of unit volume, and the above integral approximated by a sum, the $\{m_k\}$ may be regarded as the discrete equivalent of the distribution function. The quadratic nature of the original D motivates us to construct a profit function which is likewise quadratic as the nature of the optimisation problem then remains the same. Hence we have taken the profit function to be of the form

$$S = \sum_{k=1}^M \left(\frac{m_k}{p_k} - 1 \right)^2, \quad (50)$$

where the $\{p_k\}$ are specified statistical weights. In practice a reasonable choice for these is such as to give each orbit equal weight, e.g.

$$p_k = M. \quad (51)$$

Proceeding as outlined above, we form a new function D' to be minimised such that

$$D' = D + \mu S, \quad (52)$$

where μ is a small positive constant whose magnitude reflects the degree of smoothness imposed on the solution. By solving this quadratic optimisation problem the required $\{m_k\}$ for an equilibrium solution can be calculated. We use the two phase quadratic programming method of Gill et al. (1986) which is implemented in the NAG library routine E04NCF. On each orbit k we then place n particles, where n is proportional to m_k . By placing the particles at equal time intervals along each orbit we ensure a smooth distribution in orbital phase.

4.3 Application to the perfect oblate spheroid

The POSP, being a Stäckel potential, is completely integrable. Each orbit has three conserved actions associated with it making the construction of an M -orbit family on which to base our equilibrium easier. But the method can be applied to more general mass distributions, as will be seen in the next section, provided an M -orbit family can be constructed which adequately samples phase space.

As a consequence of integrability, a general orbit in the POSP separates into librations between fixed values of the u and v coordinates, so that orbits can be classified by the triple (u_+, u_-, v) where u_+, u_- are the extrema in the u coordinate and $\pm v$ the extrema in the v coordinate. In terms of a thin disc model we can think of oscillations in u and v as corresponding to radial and vertical oscillations respectively. Here we seek an equilibrium distribution which consists of stars on infinitesimally thin short-axis tube orbits (a ‘‘shell orbit’’ model). These orbits have no libration in the u direction. Thus, in the thin disc limit they correspond to circular

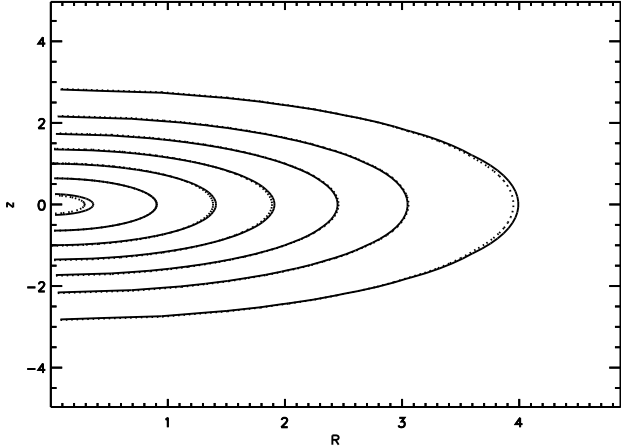


Figure 4. Comparison of the analytic density (solid line) with that of an N -body sample (dashed line) for an $e = 1$ perfect oblate spheroid.

orbits with superposed small amplitude vertical oscillations. Bishop (1987) tackled this problem via a numerical solution of the corresponding density/distribution function integral equation.

To set up an orbit family we divide the (u, v) plane into a grid which evenly samples the mass of the system and then allocate an orbit to each grid cell which has its turning points randomly allocated within the cell. These orbits are then integrated in the POSP for such a time that the $\overline{\Phi}_{l0}$ are determined to a sufficient accuracy.

Using an orbit family of 1000 orbits together with 40 of the Φ_{l0} and applying no smoothing (i.e. $\mu = 0$), a good N -body realisation of an equilibrium $e = 1$ perfect oblate spheroid (in the sense of a small value of D') is found but only around 100 orbits are occupied. However, setting $\mu = 10^{-4}$ increases the number of occupied orbits to around 800 whilst having little effect on the value of D' . A contour plot comparing the analytic density with the basis set representation of the N -body distribution (using 100K particles) is shown in Figure 4 (where the contours are logarithmically spaced).

4.4 Application to the KT disc

The orbits we use to build our KT disc from are taken by sampling one of the distribution functions used in Sellwood & Merritt (1994). They used an analytic distribution function for the planar motion (derived in Kalnajs 1976). They assigned z velocities by first integrating the one-dimensional Jeans equation for the vertical motion

$$\frac{1}{\rho} \frac{\partial(\rho\sigma_w^2)}{\partial z} = F_z \quad (53)$$

(where F_z is the vertical component of the gravitational acceleration) to find the velocity dispersion $\sigma_w(z)$, and then by assuming the vertical velocity distribution to be a Gaussian of width $\sigma_w(z)$. We generated our orbit family by sampling the distribution function in two stages. First we sampled values of R and z from the density distribution $\rho(R, z)$. Then for each particle position we sampled the velocity component

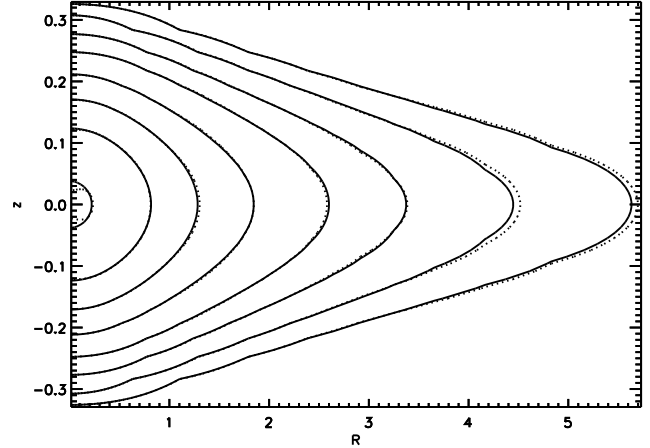


Figure 5. Comparison of the analytic density (solid line) with that of an N -body sample (dashed line) for $z_0 = 0.1$ KT disc.

perpendicular to the vertical z axis using the Kalnajs distribution function. Finally the vertical velocity component v_z was sampled from the Gaussian of width $\sigma_w(z)$, the latter having been determined from (53). Positions and velocities determined in the above manner were used to provide the initial conditions for the orbit family.

We adopted the planar distribution function which is independent of angular momentum, and hence isotropic ($m_K = 3$ in the notation of Sellwood & Merritt 1994), and take the z scale height $z_0 = 0.1$. As before an orbit family of 1000 orbits and 40 of the Φ_{l0} were used, and setting $\mu = 10^{-3}$ resulted in around 900 of these orbits being occupied. A contour plot comparing the analytic density with the basis set representation of the N -body distribution (using 100K particles) is shown in Figure 5 (again with logarithmically spaced contours).

5 EQUILIBRIUM SIMULATIONS

Our N -body simulation code uses a standard second-order time-centred leapfrog integration scheme. The forces on each particle are calculated from the basis set expansion

$$\mathbf{F}(\mathbf{r}_k) = - \sum_{l,m} c_{lm} \mathbf{F}_{lm}(\mathbf{r}_k), \quad (54)$$

where the fourier coefficients c_{lm} are calculated from the set of particle positions $\{\mathbf{r}_k\}$ via

$$c_{lm} = - \sum_{k=1}^N \Phi_{lm}(\mathbf{r}_k), \quad (55)$$

To assess the quality of our simulations, we conduct energy and angular momentum conservation tests and calculate the relaxation rate for the POS and KT disc equilibria generated in the previous section. We use 20K particles, 30 of the basis functions, and a step-size of approximately 0.004 times the dynamical time t_{dyn} of each system, where we have defined t_{dyn} to be the time for a particle at the half-mass radius of the system to complete a quarter of one circular orbit around the system. We adopt the appropriate

t_{dyn} as the unit of time in both cases. The results presented here were produced using functions generated via method a), though method b) gives similar results.

To suppress any instabilities we impose axisymmetry and reflection symmetry in the $z = 0$ plane, by omitting all $m > 0$, and z antisymmetric functions respectively from our basis set expansions. We also ran the systems for several time units before beginning the tests to allow any initial fluctuations to phase mix away. This ensures that we are testing the quality of the code, rather than discreteness effects in the initial equilibria. We give results for the simulations over a period of ten dynamical times, though we ran the systems for many more dynamical times to ensure that the results given here are typical.

Sellwood & Merritt (1994) advocated the use of a quiet start in their N -body stability studies of KT discs. One feature of their quiet start is that they allocated particles in groups obeying certain symmetries (e.g. in the z direction and in azimuthal segments). This ensures that the net linear and angular momentum of the system is zero and that low azimuthal mode numbers can be made to be absent from the initial density distribution. It also ensures that any subsequent rapid growth of such an $m \neq 0$ component can be ascribed to instabilities. However, since here we are testing axisymmetric equilibria simulations and effectively impose such symmetries on the system *ab initio* by excluding all z antisymmetric and non-axisymmetric functions from the basis expansions such a quiet start becomes redundant (except in the total momentum conservation tests). In fact we find that in this situation using a quiet start may raise the noise level and relaxation rate, since, for example, allocating particles in pairs, at phase positions $(x, y, \pm z, v_x, v_y, \pm v_z)$ effectively halves the number of particles the expansion can ‘see’ and thus raises the noise level by a factor of $\sqrt{2}$ since noise scales as $1/\sqrt{N}$.

5.1 Virial ratio

The scalar virial theorem (see, e.g. Binney & Tremaine 1987) tells us that

$$\frac{1}{2}\ddot{I} = 2KE_{\text{total}} + PE_{\text{total}}, \quad (56)$$

where

$$I = \sum_{i=1}^N |\mathbf{x}_i|^2, \quad (57)$$

$$\begin{aligned} KE_{\text{total}} &= \frac{1}{2} \sum_{i=1}^N |\mathbf{v}_i|^2, \\ PE_{\text{total}} &= -\frac{1}{2} \sum_{i,j=1, i \neq j}^N \frac{1}{|\mathbf{x}_i - \mathbf{x}_j|} \\ &= -\frac{1}{2} \sum_{l,m} c_{lm}^2. \end{aligned} \quad (58)$$

In exact steady state equilibrium with an infinite number of basis functions, the quantity \ddot{I} should be identically zero. Thus the behaviour of $-2KE_{\text{total}}/PE_{\text{total}}$ is an indication of how close our N -body systems are to true equilibrium. As shown in Figures 6 and 7 the virial ratio in both

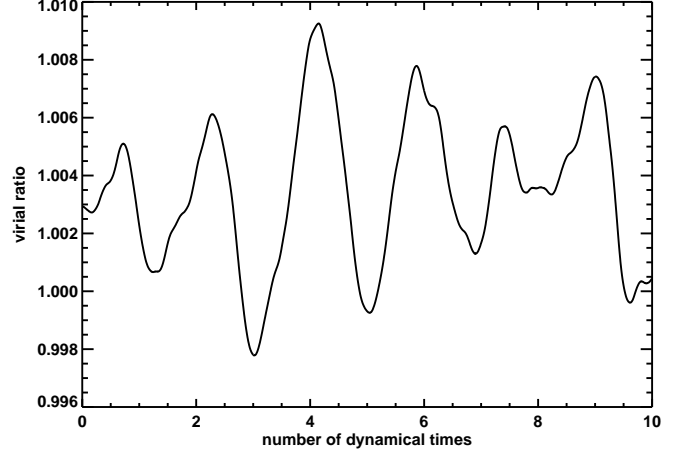


Figure 6. Evolution of virial ratio of POS equilibrium simulation.

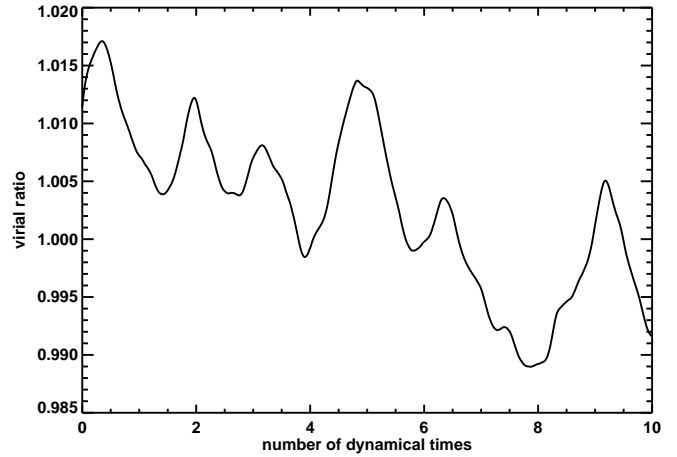


Figure 7. Evolution of virial ratio of KT disc equilibrium simulation.

systems is maintained at unity ± 0.02 which is consistent with the statistical error we would expect with $20K$ particles.

5.2 Total energy conservation

The total energy of the system is given by

$$E_{\text{total}} = KE_{\text{total}} + PE_{\text{total}}, \quad (59)$$

The fluctuation in E_{total} is less than 0.1 % in our simulations.

5.3 Relaxation

In a collisionless system, individual particle energies should be conserved. In our simulations, however, due to discreteness noise individual particle energies will tend to random walk slightly with time - i.e. the system relaxes away from the initial collisionless equilibrium. This effect is shown in Figures 8 and 9 where we plot the relative change in energy of the N particles over the duration of the test of $10t_{\text{dyn}}$

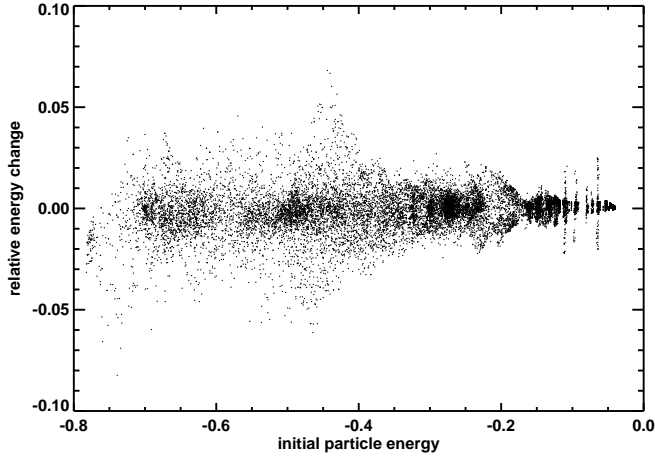


Figure 8. Individual particle energy deviations for the POS equilibrium simulation.

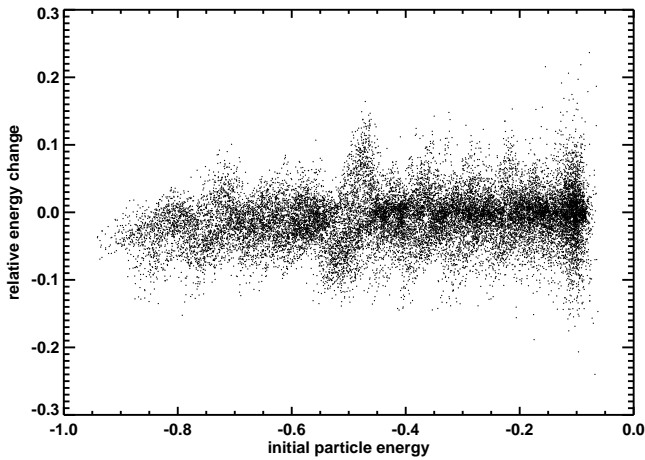


Figure 9. Individual particle energy deviations for the KT disc equilibrium simulation.

against their initial energies. The vertical band-like structure observed in these scatter plots is found in similar simulations described in Vine & Sigurdsson (1998). They state that there will be regions where the discrepancy between the value of the potential given by the basis expansion and the true value of the potential is greater than average (because of the expansion truncation), and that the bands contain the particles which occupy these regions.

To quantify the relaxation we define

$$A = \frac{1}{N} \sum_{k=1}^N \left[\frac{E_k(t) - E_k(t_0)}{E_k(t_0)} \right]^2, \quad (60)$$

where $E_i(t)$ is the energy of particle i at time t . We note that if the energies of individual particles undergo a random walk, A as well as each individual term in the summation is expected to increase linearly with time.

In Figures 10 and 11 we can see that indeed A grows linearly in time as expected. However, the rate of increase is different for the two systems. There are at least two possible explanations for this. The first is that the definition of t_{dyn}

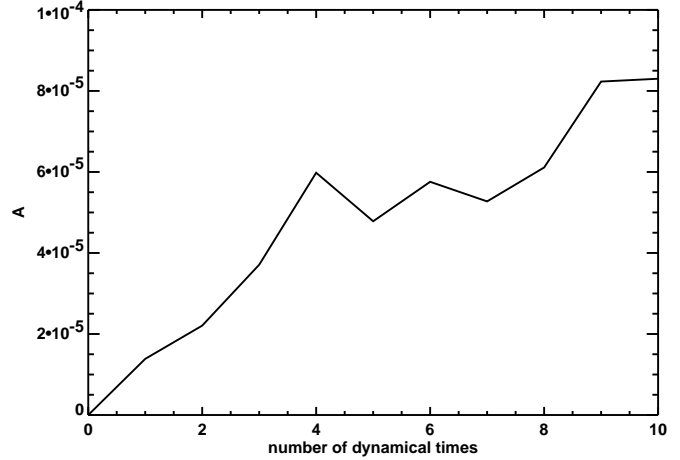


Figure 10. Relaxation of POS equilibrium simulation.

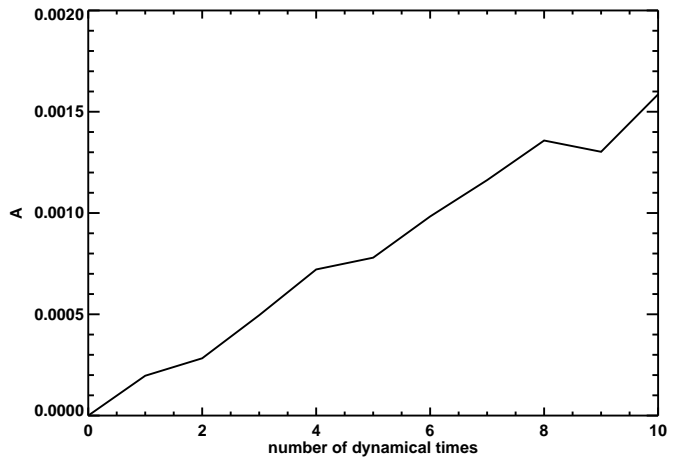


Figure 11. Relaxation of KT equilibrium simulation.

is fairly arbitrary and is only an indicator of the dynamical time-scale of the two systems, hence we may not be exactly comparing like with like. The second, which may explain why the relaxation rate of the POS simulation is smaller than that of the KT disc is due to the different nature of the orbits in the two systems. The KT disc model contains many low angular momentum, radial orbits which pass close to the centre of the system. It is likely that such orbits will suffer more relaxation on average as the centre of the system is subject to proportionately more noise disruption. With the POS “shell orbit” model fewer particles pass near the centre of the system, and the orbits are more isolated from each other in phase space, so we might expect the relaxation rate in this model to be smaller.

For the POS simulation the relaxation time is of order 10^5 times t_{dyn} , whilst for the KT disc it is of the order 10^4 times t_{dyn} , hence we can run simulations for hundreds of dynamical times before becoming too concerned about the effects of relaxation. The relaxation rate for runs using the basis set generated by method b) with $L_{\text{max}} = 30$ has about a 10% larger relaxation rate, because of the lower accuracy of the method b) functions.

Runs with different numbers of particles indicate that the relaxation rate is inversely proportional to the number of particles used, as we would expect.

We also briefly study the dependence of the relaxation rate on the number of basis functions used. A simulation using only the zeroth order basis function has a much reduced relaxation rate (by around a factor of 10), but a simulation using the first five z and axisymmetric functions has much the same relaxation rate as the original simulation which employs thirty. This effect can be understood from Weinberg (1993), which predicts that the relaxation rate of an N -body simulation code in which small scale particle fluctuations have been suppressed will be dominated by large scale modes which are generated by particle noise and amplified by self-gravity. In our results the runs with five functions adequately represent these dominant modes and additional functions contribute little to the rate of relaxation.

5.4 Linear and angular momentum

Any simulation code in which the forces are not calculated via pair-wise summation will violate momentum conservation to some degree. The drift in linear momentum can be compensated for by recentring the coordinate grid on the centre of mass of the system. By imposing suitable symmetries on the initial particle distribution its total angular momentum $\mathbf{L} = (L_x, L_y, L_z)$ is set to zero. During the simulations L_z is conserved exactly for individual particles (which is imposed by the exclusion of non-axisymmetric forces), hence total L_z is also conserved exactly. Whilst individual L_x and L_y should not be conserved, the total L_x and L_y are seen to be conserved exactly in our simulations.

6 CONCLUSIONS AND FURTHER WORK

We have shown that it is possible to numerically construct a potential-density pair basis set which is customised to a general equilibrium distribution, and demonstrated how the set can represent deviations from the original distribution with a high level of accuracy.

We have demonstrated how the set can be used to construct an N -body equilibrium sample of a density distribution without explicit knowledge of the integrals of motion of the system and without explicit reference to a known distribution function using an orbit based method. We have developed an N -body simulation code which calculates particle forces using the basis set, and have demonstrated the accuracy of the code with regards to conservation of integrals of motion and relaxation effects, and described the effect of changing the number of particles and basis functions used.

Because the basis construction is completely general, we can apply the technique to systems for which no suitable analytic basis set is known. Since the CPU time required to generate a new basis set is not prohibitive, it should also prove possible to follow the evolution of a given system even if it has evolved significantly away from its original configuration by generating a new basis set from the current density distribution.

Because the computational cost of the simulation code scales linearly with N , large numbers of particles can be

employed which will reduce the effect of particle noise resulting in more accurate simulations. There has been much discussion on the relative merits of different N -body simulation methods (e.g. Hernquist & Barnes 1990, Hernquist & Ostriker 1992, Earn & Sellwood 1995, Sellwood 1997) and it seems clear that for certain classes of problem, namely detailed studies that involve not too large deviations from an initial distribution, a basis set expansion N -body code is one of the most competitive.

We comment further that the method can be applied to problems involving two (or more) distinct mass distributions, for example a galactic disc embedded in a dark matter halo system. This involves combining the kind of axisymmetric basis set described in this paper to represent the disc distribution with a similarly generated spherical basis set to represent the halo distribution. In addition to stability studies, problems involving the warping of a galactic disc embedded in a halo, or the effects of an infalling satellite on the system can be studied. We hope to report on such work in the near future.

ACKNOWLEDGMENTS

This work was supported by PPARC grant GR/H/09454, and MJWB is supported by a PPARC studentship.

REFERENCES

- Allen, A.J., Palmer, P.L., & Papaloizou, J. 1990, MNRAS, 242, 576
 Binney, J., & Tremaine, S. 1987, Galactic Dynamics (Princeton Univ. Press)
 Bishop, J., L. 1987, ApJ, 322, 618
 Clutton-Brock, M. 1972, Ap&SS, 16, 101
 Clutton-Brock, M. 1973, Ap&SS, 23, 55
 Courant, R., & Hilbert, D. 1955, Methods of Mathematical Physics Vol I(2nd ed.; New York:Interscience Publishers)
 de Zeeuw, P. T., 1985, MNRAS, 216, 273
 Earn, D. J. D., 1996, ApJ, 465, 91
 Earn, D. J. D., & Sellwood, J. A. 1995, ApJ, 451, 533
 Gill, P.E., Hammarling, S.J., Murray, W., Saunders, M. A. & Wright, M. H., 1986, User's guide for LSSOL (Version 1.0): A Fortran package for constrained linear least-squares and convex quadratic programming. Technical Report SOL 86-1. Systems Optimization Laboratory, Dept. of Operations Research, Stanford Univ.
 Hernquist, L., & Barnes, J. E. 1990, ApJ, 349, 562
 Hernquist, L., & Ostriker, J. P. 1992, ApJ, 386, 375
 Kalnajs, A. J., 1976, ApJ, 205, 751
 Merritt, D., 1993, ApJ, 413, 79
 Press W.H., Flannery B.P., Teukolsky S.A., & Vetterling W.T., 1996, Numerical Recipes: The Art of Scientific Computing, Cambridge University Press
 Richstone, D. O., & Tremaine, S. 1988, ApJ, 327, 82
 Robijn, F. H. A., & Earn, D. J. D. 1996, MNRAS, 282, 1129
 Schwarzschild, M. 1979, ApJ, 232, 236
 Sellwood, J. A. 1997, Computational Astrophysics (ASP Conference Series)
 Sellwood, J. A., & Merritt, D. 1994, ApJ, 425, 530
 Sridhar, S., 1987, J. Astrophys. Astron. 8, 257

- Syer, D., 1995, MNRAS, 276, 1009
Syer, D., & Tremaine, S. 1996, MNRAS, 282, 223
Tremaine, S., Hénon, M., & Lynden-Bell, D. 1986, MNRAS,
219, 285
Vine, S., & Sigurdsson, S. 1998, MNRAS, 295, 475
Weinberg, M. D., 1993, ApJ, 410, 543